Development and experiments of low frequency ultrasonic electrostatic atomizing nozzle with double resonators

Jianmin Gao*, Ke Xu, Rui He, Xiangchao Chen, Mazhar Hussain Tunio

(*School of Agricultural Engineering, Jiangsu University, Zhenjiang 212013, China*)

Abstract: Fine droplets with high adhesion can greatly improve the efficiency of atomization culture. Therefore, the development of a spray nozzle that can produce fine fog droplets with high adhesion is of great significance for aeroponics. Compared to piezoelectric ultrasonic atomizer, Hartmann resonator low-frequency ultrasonic electrostatic atomizer has the advantages of large atomization volume and constant liquid chemical structure, but the droplet size is larger. High-speed gas can generate low-frequency ultrasonic vibration sound waves in Hartmann resonator. The frequency and intensity of sound waves determine the atomization performance of supersonic atomizer nozzle. However, very few research literatures can be found on how the structure and operating parameters of Hartmann resonator affect the atomization performance. In order to improve the atomization performance of ultrasonic atomizer, a two-stage Hartmann resonator low-frequency ultrasonic electrostatic atomizer was designed. The shrinkage-type Laval tube was designed by fluid mechanics theory, and the design results were verified by fluent software. The virtual orthogonal test method was used to optimize the structure parameters of two-stage resonator and spray test was carried out. The results showed that when the included angle between the two stage resonators was 80°, the diameter was 4.86 mm, the tube length ratio was 1.0 and the gas pressure was 0.5 MPa, the droplet size could reach 22.05 μm. Additionally, compared with the traditional Hartmann cavity with 90 ° included angle, the droplet size was decreased by 63%. The annular electrode was used as the charging electrode, and Comsol Multiphysics software was used to simulate and calculate the deformation and crushing process of electrostatic droplets and the influence of different voltage, surface tension and droplet diameter on the droplet deformation rate. The results showed that: (1) the optimum charge range of the electrode ring was within 20 mm of the axial distance along the electrode ring. (2) The higher the voltage U, the smaller the surface tension σ; the larger the droplet diameter d and the larger the droplet deformation rate. (3) The experimental results showed that the droplet size was inversely proportional to the gas pressure P_0, electrostatic voltage U and spray height h. When the gas pressure and electrostatic voltage were 0.4 MPa and 18 kV, 0.4 MPa and 18 kV, respectively, the droplet sizes were 7.8 μm and 43.9 μm respectively, the droplet size difference between the two conditions was 82.2%.

Keywords: ultrasonic atomization, Laval tube, two-stage resonance tube, electrostatic spray, deformation rupture, simulation analysis

DOI: 10.25165/j.ijabe.20221504.6251

Citation: Gao J M, Xu K, He R, Chen X C, Tunio M H. Development and experiments of low frequency ultrasonic electrostatic atomizing nozzle with double resonators. Int J Agric & Biol Eng, 2022; 15(4): 39–48.

1 Introduction

The spray droplet with high adhesion can greatly improve the efficiency of atomization culture[1-4]. Compared with other atomization methods, ultrasonic atomization produces fine and uniform droplets, which has natural advantages in the formation of fine droplets[5-11]. At present, ultrasonic atomization mainly includes piezoelectric ultrasonic atomization and pneumatic ultrasonic atomization. Shiau et al.[12,13] concluded that the piezoelectric atomization had a great influence on the pH, EC and chemical properties of the nutrient solution during the process of atomizing nutrient solution, which brought more results that are more uncertain for atomizing culture. The pneumatic ultrasonic atomizer produces low-frequency ultrasonic vibration in Hartmann cavity through supersonic gas to atomize the liquid. Compared with the piezoelectric ultrasonic atomizer, the pneumatic ultrasonic atomizer has a large atomization volume and does not change the composition of the nutrient solution, but the droplet size is larger. To promote the development of atomization cultures it is important to study the generation of high adhesion fine droplets from pneumatic ultrasonic atomizers.

Rayleigh et al.[14] has long studied the deformation and breakage of charged droplets in the process of electrostatic spraying. They believed that the charge carried by electrostatic droplets must tend to a constant value, and when the constant value is exceeded, the droplets will break apart, it is called the Rayleigh limit. Liu et al.[15] designed a gas-assisted electrostatic induction nozzle, it mainly consists of a nozzle body, a nozzle plate, a ring electrode, an inlet pipe and a nozzle cap. The electrostatic atomization process aims to atomize the liquid flow by the impact of the high-speed airflow and to further refine it under the influence of the electric field generated by the annular electrode at the outlet. This nozzle can effectively reduce the droplet size and achieve directional atomization. Gao et al.[16] designed a Hartmann low-frequency ultrasonic atomizing nozzle with a stepped resonator and used the acceleration principle of Laval tube and the resonance

Received date: 2021-10-26 **Accepted date:** 2022-03-24

Biographies: Ke Xu, Master candidate, research interests: air tilling, Email: 1622922822@qq.com; **Rui He**, Master, research interests: air tilling, Email: 1787381877@qq.com; **Xiangchao Chen**, Master, research interests: air tilling, Email: 2541481918@qq.com; **Mazhar Hussain Tunio**, PhD candidate, research interests: soilless cultivation systems, agricultural engineering, Email: mazharhussaintunio@sau.edu.pk.

***Corresponding Author: Jianmin Gao**, Professor, research interests: soil and air tilling. No.301 Xuefu Road, Zhenjiang 212013, Jiangsu Province, China. Tel: +86-13655282069, Email: gaojianminujs@163.com.

performance of the resonator to atomize the liquid flow. The advantages of this nozzle are small droplet size, large spray range and long spray distance[16]. Hou[17] designed a copper foil type electrostatic spray for agriculture atomization, by using the method of droplets deposition experiment. He analyzed the charged droplets electro-deposition effect without charge, and the experimental results showed that using the electrostatic spray technology could increase the deposition rate of the front side of cloud droplets in crops, have certain effect on diseases and pests prevention[17]. Li and Liang et al.[18,19] studied the process of electrostatic droplet deposition and deformation and crushing.

In order to generate fine droplets with high adhesion, this article intends to design a low-frequency ultrasonic atomizer with large atomization volume by developing a hydrodynamic low-frequency ultrasonic atomizer based on electrostatic atomization technology.

2 Overall structural design of air-assisted electrostatic ultrasonic atomizing nozzle

The structural diagram of air-assisted electrostatic ultrasonic atomizing nozzle is intended in Figure 1. It is mainly composed of Laval tube, two-stage resonance tube and electrostatic induction ring. The atomization step consists of three parts: first, the air -flow into the nozzle accelerates to supersonic speed through the Laval tube and then meets the liquid flowing into the inlet, so that the liquid atomizes under the impact of the high-speed air-flow. Secondly, the high-speed airflow flows into the resonant cavity, and the reciprocating motion in the resonant cavity produces high-frequency vibration, so the liquid flowing through this process was broken again under the action of ultrasonic wave. In the last, when the droplets were ejected from the nozzle, the particle size of the droplets was more refined under the combined action of high voltage electrostatic field and airflow field. The spray droplets produced by the nozzle can effectively improve the spray culture efficiency and meet the demand of plants for nutrient solution.

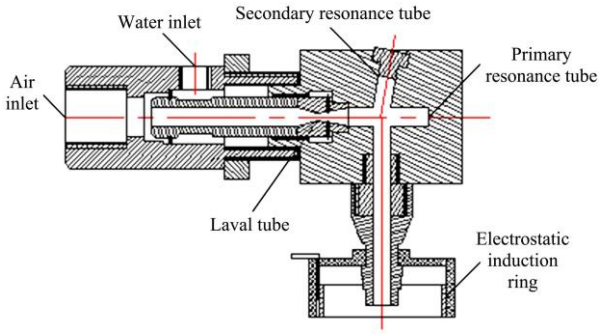

Figure 1 Structural diagram of air-assisted electrostatic ultrasonic atomizing nozzle

3 Design of Laval tube structure

3.1 Determination of structural parameters of Laval tube

Laval tube is a type of gas accelerator. The design of the Laval tube is mainly composed of four parts: stability section, contraction section, transition section and expansion section. The theoretical work is based on[20-22]

$$\frac{\mathrm{d}S_A}{S_A}=(M^2-1)\frac{\mathrm{d}v}{v} \tag{1}$$

where, M is the fluid Mach number; S_A is the cross-sectional area of passage, m^2; v is the airflow velocity, m/s.

It can be seen from Equation (1) that when the right side of the formula is greater than 0, that is $M>1$, v increases with the increase of S_A. When $M<1$, v decreases with the increase of S_A, and v increases with the decrease of S_A. In other words, when the fluid velocity is greater than the speed of sound, the fluid velocity increases as the cross-sectional area of the pipe increases, and decreases when the cross-sectional area of the pipe decreases. Furthermore, when the fluid velocity is less than the speed of sound, the fluid velocity decreases when the cross-sectional area of the pipe decreases and vice versa. From the above theoretical analysis, it is concluded that in order to achieve supersonic flow at the outlet of Laval tube, the cross-sectional area of Laval tube should be reduced first and then increased, additionally, the cross-sectional area should be kept unchanged in the transition part, it is named as the throat part.

The main design dimensions of Laval tube are inlet diameter d_1, throat diameter d_0, outlet diameter d_2, contraction angle α, and expansion angle β. The schematic diagram of Laval tube designed in this paper is shown in Figure 2.

The gas flow in Laval tube belongs to one-dimensional non-viscous isentropic flow and the flow process satisfies:

$$\frac{\mathrm{d}p}{p}=-\gamma M^2\frac{\mathrm{d}v}{v} \tag{2}$$

$$\frac{\mathrm{d}T}{T}=-(\gamma-1)M^2\frac{\mathrm{d}v}{v} \tag{3}$$

where, v is the velocity of the gas, m/s; p is the gas pressure, MPa; T is the gas temperature, K; M is the Mach number; γ is the adiabatic index.

Since the flow velocity in Laval tube is a process of gradual increase, namely $\mathrm{d}v/v>0$, it can be obtained from the above equation that $\mathrm{d}p/p<0$, $\mathrm{d}T/T<0$, and the pressure and temperature of the gas in Laval tube gradually decrease.

According to the calculation formula of the throat area of Laval tube[14]:

$$A_0=\frac{Q_0\sqrt{T_1}}{P_1\sqrt{\frac{\gamma}{R}\left(\frac{2}{\gamma+1}\right)^{\frac{\gamma+1}{\gamma-1}}}} \tag{4}$$

where, A_0 is the throat section area of Laval tube, m^2; Q_0 is the mass flow of air at the Laval pipe inlet, kg/s; T_1 is the temperature at the entrance of the Laval tube, K; P_1 is the pressure at the entrance of Laval tube, MPa; R is the gas constant, J/(kg·K); γ is the adiabatic index.

Formula for calculating outlet area of Laval tube[23]:

$$Q_0=A_2\left(\frac{p_2}{p_1}\right)\frac{1}{\gamma}\sqrt{\frac{2\gamma}{\gamma-1}\rho_1 p_1\left[1-\left(\frac{p_2}{p_1}\right)^{\frac{\gamma-1}{\lambda}}\right]} \tag{5}$$

where, A_2 is the sectional area of Laval tube outlet, m^2; Q_0 is the mass flow of air at the Laval pipe inlet, kg/s; P_1 is the pressure at the entrance of Laval tube, MPa; P_2 is the pressure at the Laval outlet, MPa; ρ_1 is the gas density at the entrance of Laval tube, kg/m^3; R is the gas constant, J/(kg·K); γ is the adiabatic index.

It is known that the mass flow Q_0 at the inlet of Laval tube is 5.08×10^{-3} kg/s, when the gas pressure P_1 at the inlet of Laval tube is 0.3 MPa, the gas density ρ at the inlet is 3.53 kg/m^3, T_1 is 300 K, the adiabatic index γ is 1.41, and the gas constant R is 286.8 J/(kg·K). From Equations (2) and (3), it can be concluded that the throat diameter d_0 of Laval tube is 2.1 mm, and the outlet diameter d_2 is 3.4 mm. During the experiment, in order to ensure the stable and even flow from the air compressor outlet into the Laval tube in the nozzle, the inlet diameter of Laval tube was kept as large as possible, so the inlet diameter of Laval tube $d_1=3d_0$,

hence d_1 = 6.3 mm. For the convenience of processing and experience of our research group, the curve types of the contraction section and expansion section of Laval tube are straight lines, with the contraction angle α at 30 °and the expansion angle β at 10 °.

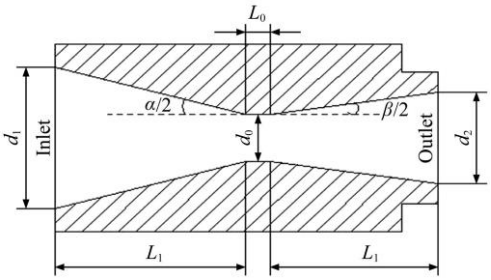

Figure 2 Structural diagram of Laval tube

3.2 Simulation of flow field in Laval tube

Auto-cad software was used for two-dimensional modeling and fluent software was used for grid generation, as shown in Figure 3. The mesh size of the entire model is 10 235, the minimum mesh size of the Laval tube throat region is 0.13 mm, and the mesh size of other parts is 0.3 mm. It selected the Realizable k-ε turbulence model by using the coupled solver SIMPLE algorithm. The model inlet boundary can be defined as the pressure, and inlet pressure is 0.3 MPa. The outlet boundary is defined as the pressure for export and takes appropriate values, the conditions for the corresponding turbulent wall processing with standard wall functions. The distribution of velocity, pressure and temperature in Laval tube are presented in Figures 4-6.

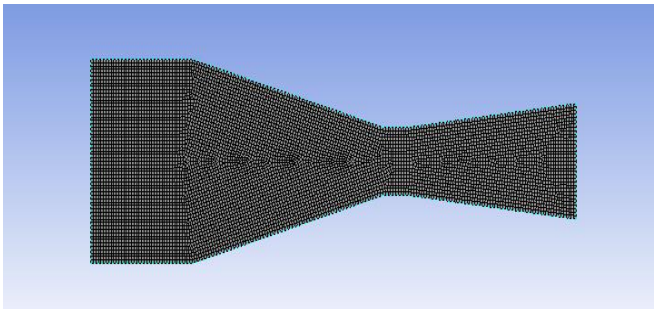

Figure 3 Meshing diagram

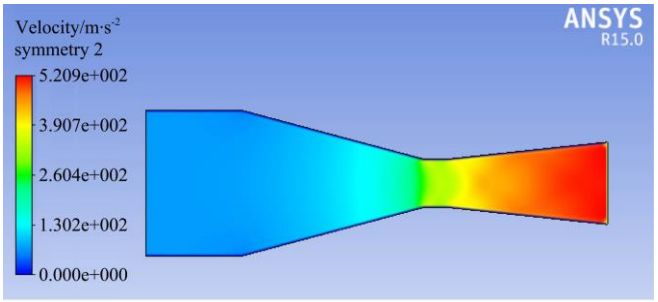

Figure 4 Velocity nephogram

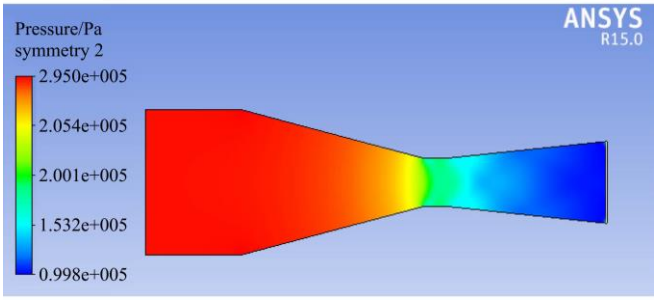

Figure 5 Pressure nephogram

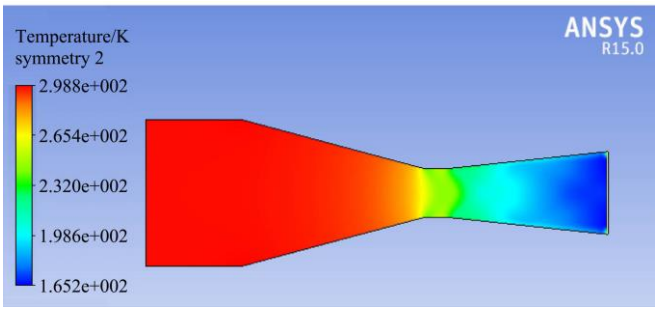

Figure 6 Temperature nephogram

It can be seen from Figures 4-6 that the gas velocity in the Laval tube gradually increases and reaches 520 m/s to the outlet, meeting the requirements of supersonic speed, the gas temperature (Figure 7a) and pressure (Figure 7b) are showing a decreasing trend, which is consistent with the theoretical analysis mentioned above.

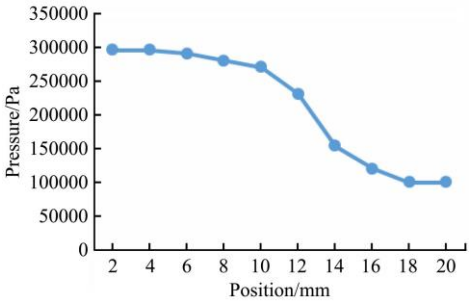

a. Pressure

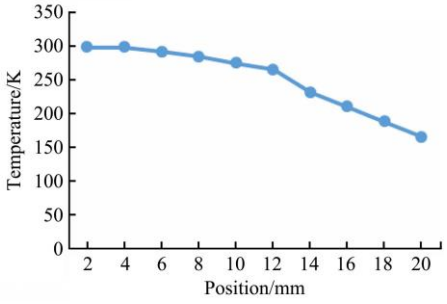

b. Temperature

Figure 7 Parameters of central axis and wall surface

4 Structure design of two-stage resonant tube based on CFD orthogonal test

4.1 Two-stage resonant tube structure design

A two-stage resonant tube was designed based on the resonance mechanism of Hartmann resonator. The specific structural diagram of two-stage resonant tube is shown in Figure 8. The main parameters included the length L_1 of the first-stage resonant tube, the length L_2 of the second-stage resonant tube, the diameter d of the resonant tube and the angle θ of the two-stage resonant tube. The main working principle is that the two-stage compression wave enters into the resonance tube. Moreover, when it spread to the secondary resonance tube a wave was generated and rebound. The rebound of the rarefaction wave in pipe mouth continued to spread to the tube; when the rebound and compression wave is generated. However, the primary resonance tube compression wave resonance affects the droplets in the two levels of vibration under the action of atomization of the resonance tube. Therefore, the resonant frequency can be used to judge whether the resonant tube has good resonant performance or not.

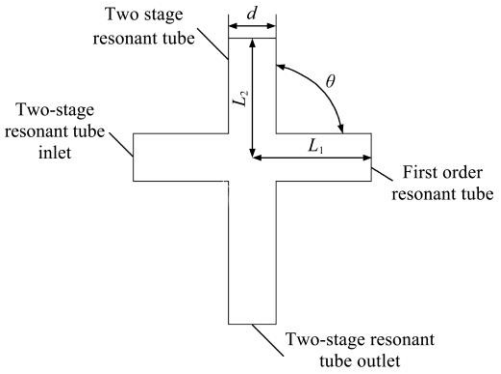

Figure 8 Schematic diagram of two-stage resonant tube structure

4.2 Calculate the setting of model and boundary condition

The fluent software was used to study the gas flow in the resonant tube[24]. The resonant frequency of the resonant tube was analyzed by using numerical simulation results and the structural parameters of the resonant tube. The designed sprinkler head was simplified and the sprinkler head flow field model was established as shown in Figure 9, where d_1 and d_2 are the inlet and outlet diameters of Laval tube, d_0 is the throat diameter, d is the diameter of the resonant tube, L_1 and L_2 are the lengths of the primary and the secondary resonant tubes respectively.

The boundary conditions of the complete model were defined the inlet as pressure inlet, and the outlet as pressure outlet. Moreover, the pressure at inlet and outlet was 0.2 MPa and 0.1 MPa respectively, and the wall was defined as the non-slip boundary condition. As shown in Figure 10, the built of two-dimensional model was imported into fluent software and mesh was divided in the mesh module. Quadrilateral supremacy was used to divide the mesh. The mesh size for the throat region of Laval tube was defined as 0.08 mm, the mesh size of other parts was 0.3 mm, and the total number of meshes was 15 432.

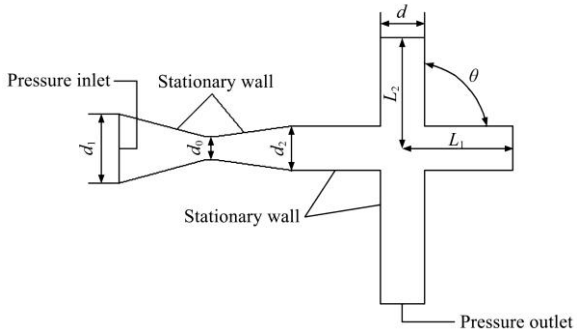

Figure 9 Calculation area of nozzle flow field model

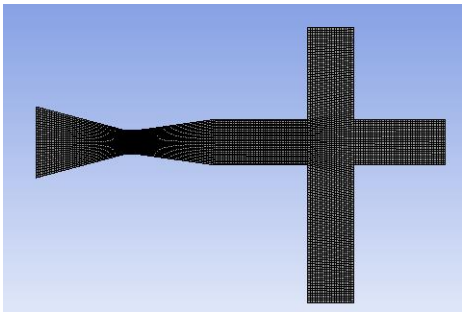

Figure 10 Diagram of meshing

The transient simulation was performed in Ansys15.0, and the density method was chosen to solve the problem, and the ideal gas was chosen as the medium material. Regardless of the heat transfer during the solution process, the Realizable k-ε turbulence model was used. The coordinates of the monitoring point P were 24.648, –5.331, and 0. The upper end of the inlet of Laval tube was taken as the origin of coordinates. The flow direction at the inlet of the whole nozzle model was on X-axis and the opposite direction of the outlet flow was on Y-axis. In this study, the simulation time and time step were set as 6000 s and 2×10^{-7} s, respectively, and the number of iterations under each time step was set to 15.

4.3 Design of orthogonal test scheme

Whether the resonant tube had good resonance performance is a key factor to measure the atomization effect of air-assisted electrostatic ultrasonic atomization nozzle and the resonance frequency f can well represent the significance of resonance state. By using fluent software combined with the method of orthogonal test[25], the transient numerical simulation of fluid flow in the two-stage resonant tube was carried out. The structural parameters of the resonant tube were determined with the help of numerical simulation results. During the process of entire test angle θ, diameter d and the pipe length ratio L_1/L_2 were selected. However, three factors for the test and for each factor four levels were selected as shown in Table 1. Additionally, the investigation index was resonance frequency f.

Table 1 Test factor level table

Level	Factor		
	Angle of two-stage resonance tube θ/(°)	Resonant tube diameter d/mm	Two-stage resonance tube length ratio L_1/L_2
1	30°	3.86	1
2	60°	4.36	1.5
3	80°	4.86	2
4	90°	5.36	2.5

It could be seen from Table 1 that this experiment is consist of three-factors and four-level test and the interaction between various factors are not considered. Therefore, $L_{16}(4^5)$ orthogonal table was selected, the two empty columns showed as the test error. The corresponding frequency spectrum diagram of the monitoring point P is shown in Figure 11. The resonance frequency of different structural parameters was compared, analyzed, and the optimal structural parameters were selected.

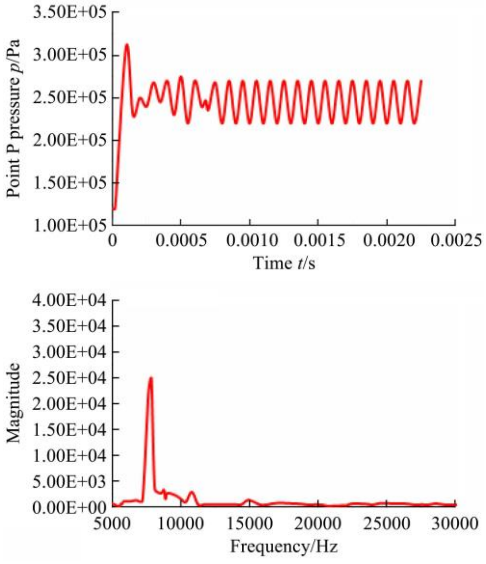

Figure 11 P point pressure time map and corresponding spectrogram

4.4 The range analysis of orthogonal test results

The fluent simulation software was used to conduct transient numerical simulation of the flow field in the resonant tube

combined with the simulation process as mentioned above. During the test, the length of the secondary resonant tube was 2*d*. The test data was statistically analyzed and range analysis was performed. The analyzed results are listed in Table 2.

Table 2 Orthogonal test range analysis results

No.	Factors			Resonant frequency *f*/Hz
	A: Angle of two-stage resonance tube θ/(°)	B: Resonant tube diameter *d*/mm	C: Two-stage resonance tube length ratio L_1/L_2	
1	1(30)	1(3.86)	1(1)	7846.8
2	1	2(4.36)	2(1.5)	7221.8
3	1	3(4.86)	3(2)	7196.3
4	1	4(5.36)	4(2.5)	5960.2
5	2(60)	1	2	9111.0
6	2	2	1	9338.1
7	2	3	4	8576.1
8	2	4	3	8766.0
9	3(80)	1	3	11268.7
10	3	2	4	11268.7
11	3	3	1	12600.3
12	3	4	2	11979.7
13	4(90)	1	4	9357.8
14	4	2	3	11253.0
15	4	3	2	11255.8
16	4	4	1	11257.7
K_{1n}	28225.1	37584.3	41042.9	
K_{2n}	35791.2	39081.6	39568.3	
K_{3n}	47117.4	39628.5	38484	
K_{4n}	43124.3	37963.6	35162.8	
k_{1n}	7056.3	9396.1	10260.7	
k_{2n}	8947.8	9770.4	9892.1	
k_{3n}	11779.4	9907.1	9621	
k_{4n}	10781.1	9490.9	8790.7	
R	4723.1	511	1470	

The order of factors affecting the resonant frequency *f* from main to secondary is as follows: angle θ of the two-stage resonant tube, the length ratio of the two-stage resonant tube L_1/L_2, and the diameter of the resonant tube *d*. The trend diagram of experimental factors and indicators is shown in Figure 12. It can be seen from Figure 12 that when the included angle of the two-stage resonant tube was 80 °, the diameter *d* was 4.86 mm and the length ratio of the two-stage resonant tube L_1/L_2 was 1. Therefore, the resonant frequency *f* of the resonant tube was the highest and the resonance performance was the best. This is the optimal scheme A3B3C1.

5 Selection of charging electrode for air-assisted electrostatic ultrasonic atomizer nozzle

More importantly, charging electrode is the key component of electrostatic system for air-assisted electrostatic ultrasonic atomizing nozzle. In this paper, based on the principle of electrostatic induction, a round tubular electrode was selected to generate an induced electric field through the electrode[26]. The material used in the electrode was copper, and it is connected with the nozzle through an insulating support frame. The specific structure is intended in Figure 13. The distance s between the axial edge of the electrode and the nozzle outlet was 12 mm, the radius *r* of the electrode ring was 20 mm, the length *l* of the electrode ring was 16 mm, and the distance *s*' between the electrode ring and the outlet of the resonator cavity was 40 mm.

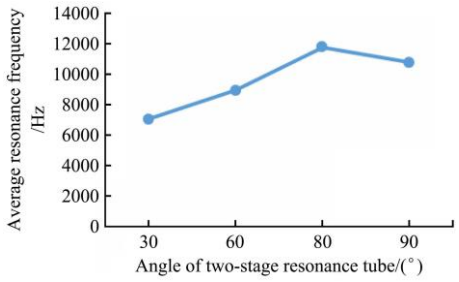

a. Angle of two-stage resonance tube

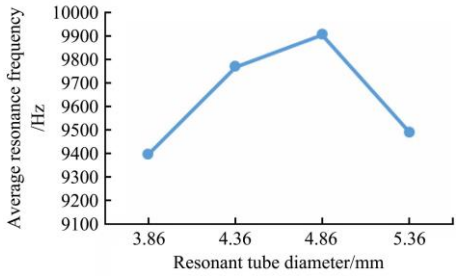

b. Resonant tube diameter

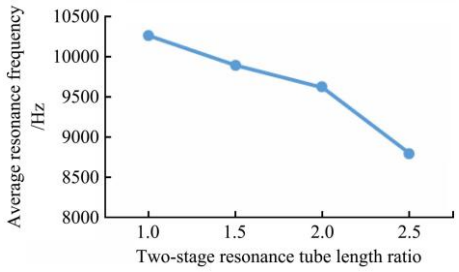

c. Two-stage resonance tube length ratio

Figure 12 Trend chart of relationship between factors and levels

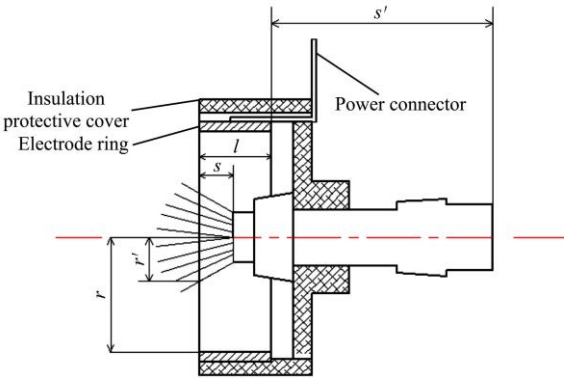

Figure 13 Electrode ring structure

6 Simulation of deformation and crushing process of electrostatic droplets

6.1 Establishment of water drop model

Additionally, charged droplet atomization refers to that under the action of electric field, a large amount of charge accumulates on the surface of droplet due to polarization. Due to the action of Coulomb force between charges, the surface tension of droplet decreased, resulting in deformation of droplet and finally breaking up into small droplets[27]. Comsol Multiphysics, a multi-physical field coupling analysis software was used to conduct numerical simulation of the deformation and crushing process of droplets, and the effects of electrostatic voltage, surface tension and droplet size on droplet deformation rate were analyzed[28]. The two-dimensional model was established for simulation analysis as shown in Figure 14. The dispersed phase water droplet was round with a diameter of 4 mm and located in the middle of the plate. According to the

single definition of static physical boundary module, plate voltage U_0 and plate under the ground were set for electrical insulating plate. The upper and lower wall and left and right wall velocity v was set to 0, as presented in Figure 15, which is showing meshing calculation model. It could be seen that the dividing unit structure mainly adopts triangle, interface, and droplets are part of the grid in encryption processing; the total grids are 28 743.

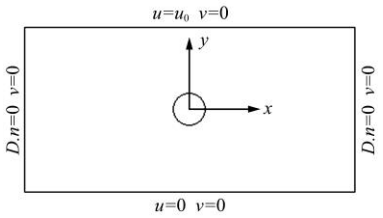

Figure 14 Physical model and boundary conditions

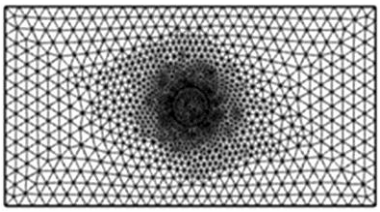

Figure 15 Grid distribution diagram

The parameters of the two phases in the model are listed in Table 3.

Table 3 Physical parameters of two substances

Substance	Density /kg m^{-3}	Viscosity /MPa s	Conductivity /S m^{-1}	Relative dielectric constant
Water	998	1	1.75×10^{-5}	80
Air	1.29	1810	0	1.000585

6.2 Analysis of deformation and crushing results of fog droplets

The deformation diagram of water droplets from t=0 ms to t=30 ms was obtained through simulation, as shown in Figure 16. It can be seen from the figure that the shape variable of water droplets under the action of electric field charge increases. When t=0 ms, the shape of water droplets is circular. With the accumulation of time, the water droplets gradually become elliptic along the axial distance, and the deformation increases in turn along the direction of the electric field. At t=22 ms, the axial deformation of the water drop reaches the maximum limit. At t=2 ms and t=4 ms, the water drop maintains the original circular state with insignificant deformation. At t=30 ms, the water drop breaks.

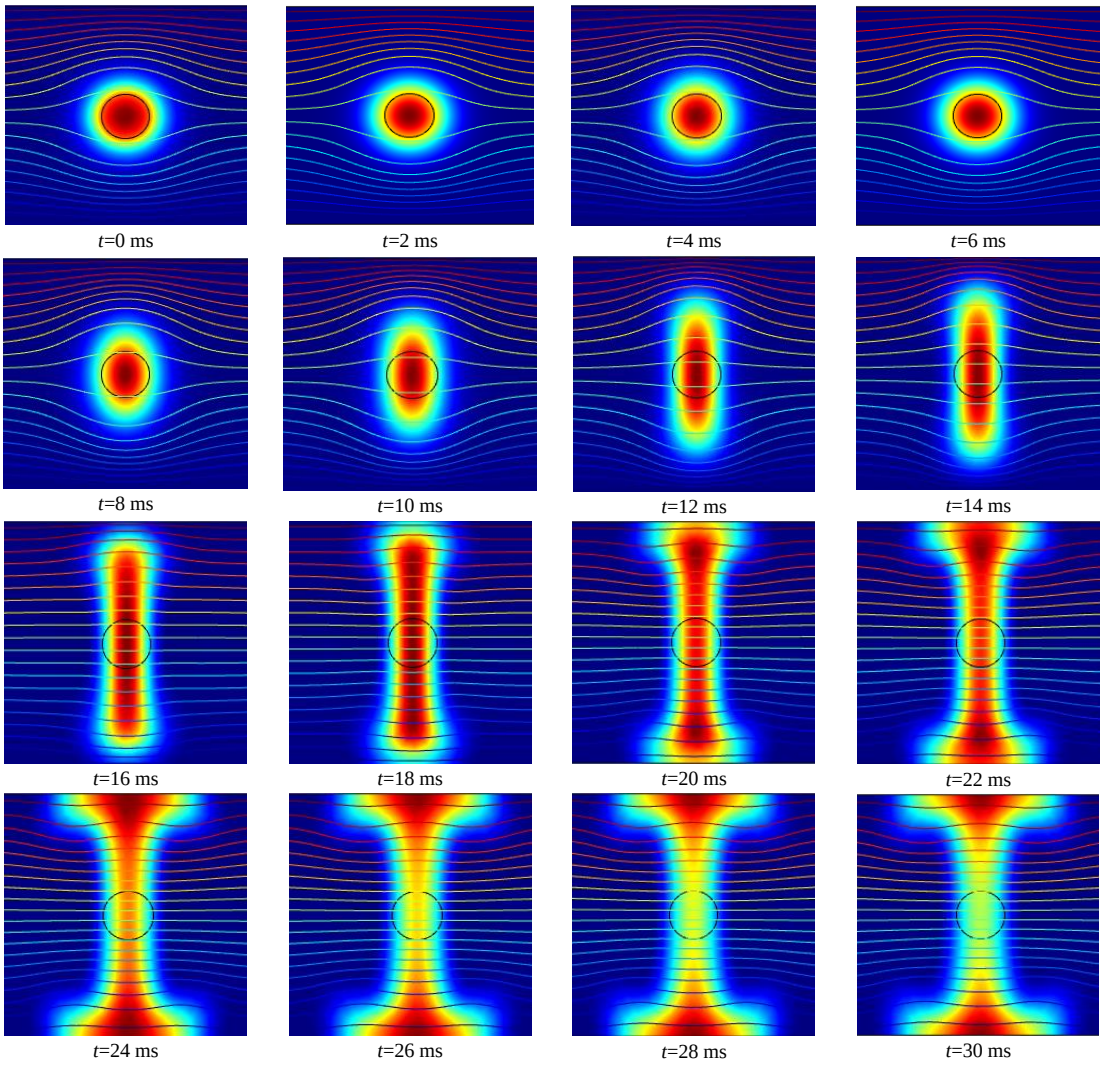

Figure 16 Deformation diagram of water droplets

6.3 Main factors that affect the deformation and crushing of water droplets

To determine the deformation amount of water droplets, it can be analyzed according to specific parameter values, as shown in Figure 17. The deformation rate of water droplets[29] is defined as:

$$D=\frac{a-b}{a+b} \tag{6}$$

where, a is the length and diameter of elliptical water droplets after deformation, m; b is the short diameter of elliptical drop after deformation, m.

Simulation parameters are listed in Table 4.

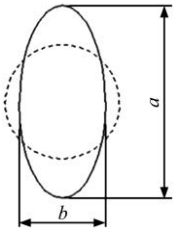

Figure 17 Deformation of water drops

Table 4 Operating conditions parameters

Serial number	Voltage U/kV	Surface tension coefficient σ/N m^{-1}	Drop diameter d/mm
1	8	0.069	4
2	10	0.071	6
3	12	0.073	8
4	14	0.075	10

6.3.1 Voltage

Under the electrostatic field, the electric field intensity had the greatest influence on the deformation rate of water droplets. It is therefore; by applying voltage, the electric field intensity was determined. According to the simulation results, when $t=4$ ms and the voltages U were 8 kV, 10 kV, 12 kV, and 14 kV, respectively, the deformation of water droplets is shown in Figure 18. Moreover, the deformation of water droplets with diameter d of 5 mm and 6 mm under different voltage U was simulated, and the relationship between the deformation rate of water droplets and the voltage is shown in Figure 19. According to Figures 18 and 19, the applied voltage U was greater than 12 kV, the deformation rate of the water drop was not particularly obvious. The main reason was that when the voltage U increased to a certain value, the electric field force received by the water drop was enough to overcome the surface tension received by the water drop, causing to break the water drop.

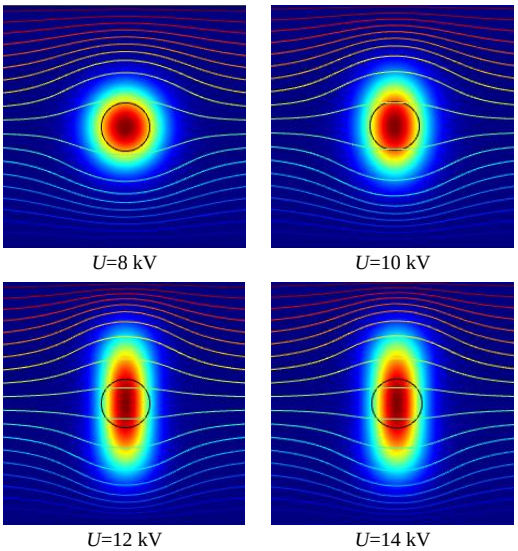

Figure 18 Deformation of water droplets at different voltages at t=4 ms

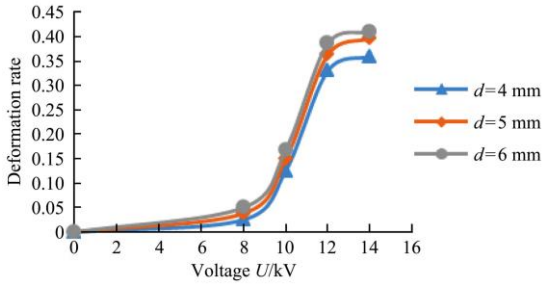

Figure 19 Relationship between water droplet deformation and electric field strength at t=4 ms

6.3.2 Surface tension

The main effect of surface tension on water droplets is to make them in a circular state, while the ratio of electric field force to surface tension has a certain influence on the deformation rate of water droplets under the action of electric field. According to the simulation results, when the voltage U=8 kV and t=4 ms, the surface tension σ was 0.075 N/m, 0.073 N/m, 0.071 N/m and 0.069 N/m. The deformation of water droplets is depicted in Figure 20. The influence of surface tension on deformation rate under different voltages was simulated, and the relation between surface tension and water droplet deformation was obtained (Figure 21). According to Figures 20 and 21, surface tension σ is inversely proportional to deformation rate of water droplets. Under the same applied voltage U, the deformation rate of water droplets decreased with the increase of surface tension σ. The main reason for the effect of surface tension on the water droplet was to maintain the water droplet in a circular state. Under the action of electric field, the electric field force causes the water

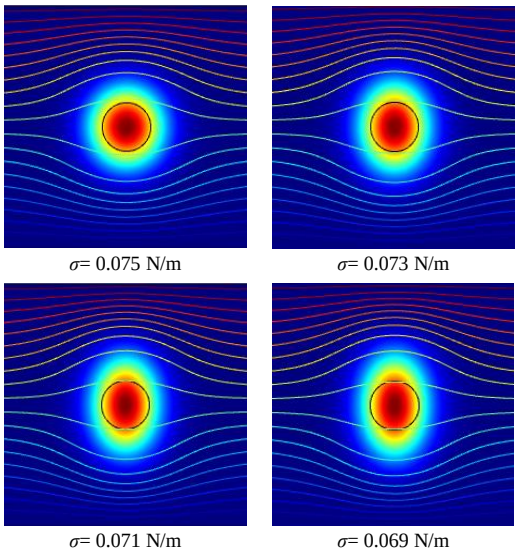

Figure 20 Deformation of water droplets under different surface tension coefficients at t=4 ms

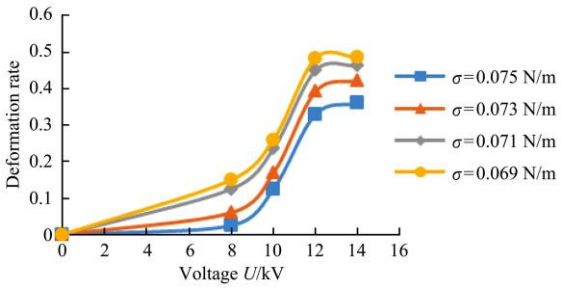

Figure 21 Relationship between different surface tension and water droplet deformation at t=4 ms

droplet to produce tensile deformation along the axial direction. Therefore, under the same applied voltage U, the smaller the surface tension, the greater the electric field force was visible on the tensile shape.

6.3.3 Droplet diameter

In other case when the applied voltage U was 8 kV and the surface tension σ was 0.075 N/m, different droplet diameters d also affected the deformation degree. The deformation diagram of droplets with diameters of 4 mm, 6 mm, 8 mm and 10 mm at t = 4 ms was obtained by simulation, as shown in Figure 22. The influences of droplet diameter on deformation rate under different voltages were simulated, and the relation between droplet deformation and droplet diameter was obtained as shown in Figure 23. According to Figures 22 and 23, under the same applied voltage U, the droplet deformation rate was directly proportional to the droplet diameter d, with the increase of droplet diameter d, the droplet deformation rate increases gradually. The main reason is that the larger the diameter d, the more the surface induced polarization charge is under the action of electric field, and the greater the action of electric field force, the greater the deformation rate.

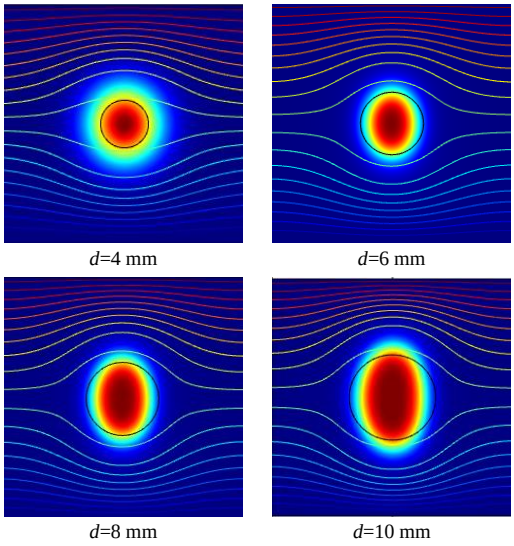

Figure 22 Deformation of water droplets at different diameters at t=4 ms

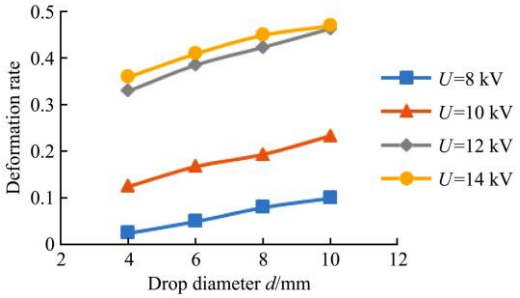

Figure 23 Deformation diagram of different diameters and water droplets at t=4 ms

7 Droplet size test

7.1 Experimental equipment and scheme

The air-assisted electrostatic ultrasonic atomizer designed in this paper is mainly used in the field of atomization cultivation, and the atomization performance of the sprinkler (droplet size) has a direct impact on the cultivation, so the droplet size of the sprinkler under different gas pressure, electrostatic voltage and spray height was tested.

The equipment used in the experiment mainly included: air compressor (Model 750-30, Shanghai Jaguar Compressor Manufacturing Co., Ltd), high voltage static electric appliance (Model KEF00-JD10060), electrostatic spray host (Model KEF00-JD10063), and air-assisted electrostatic ultrasonic atomizing nozzle generator system. Moreover, for the measurement of droplet size the Laser particle size analyzer (Model Winner318-b, Jinan Winner instrument Co., Ltd) were used. The experiment was conducted in the College of Agricultural Equipment Engineering, Jiangsu University. The temperature outside the experimental room was 27 ℃-29 ℃ and the relative humidity was 50%. The experimental medium was tap water. The entire droplet size test system is shown in Figure 24.

The test scheme is as follows: the average droplet size was tested at different spray heights (0.4 m, 0.6 m, 0.8 m, and 1 m), different electrostatic voltage (0 kV, 3 kV, 6 kV, 9 kV, 12 kV, 15 kV, and 18 kV) and different gas pressures (0.2 MPa, 0.25 MPa, 0.3 MPa, 0.35 MPa, and 0.4 MPa).

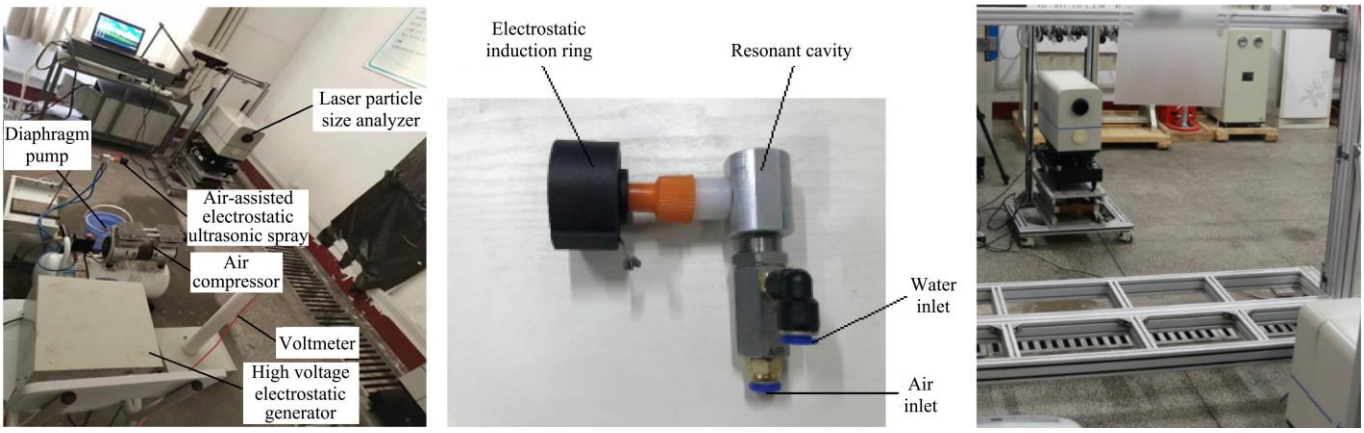

a. Droplet size test site of air-assisted electrostatic ultrasonic atomizing nozzle

b. Air-assisted electrostatic ultrasonic atomization nozzle

c. Laser particle size analyzer

Figure 24 Droplet particle size test system diagram

7.2 Test results and analysis

7.2.1 Effects of different gas pressure and electrostatic voltage on droplet size

The spray height h was fixed at 1 m, and the droplet size under different gas pressure P_0 and electrostatic voltage U was tested. The test results are shown in Figure 25. The results show that the droplet size decreased both the gas pressure P_0 and electrostatic voltage increased. When the gas pressure and electrostatic

voltage increased to 0.4 MPa and 18 kV respectively, the droplet size reached to the minimum value of 7.8 μm. The main reason for droplet size reduction is that the increase of gas pressure P_0 leads to the increase of gas velocity, which further breaks the droplet into smaller droplet under the impact of high-speed airflow. When the electrostatic voltage U applied, the electrostatic field generated by the electrostatic voltage U causes the droplets to be charged, and the charged droplets are further broken under the action of the electric field force and the Coulomb force, resulting in more smaller droplets.

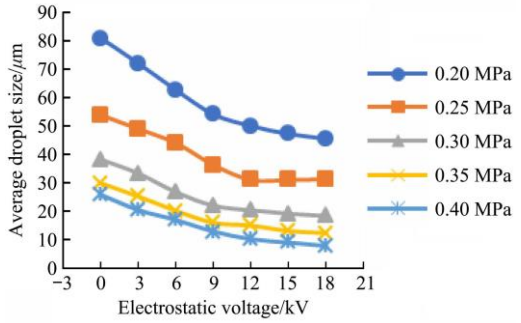

Figure 25 Variation of droplet size under different gas pressures and electrostatic voltages

7.2.2 Effects of different spray height and electrostatic voltage on droplet size

The gas pressure P_0 was fixed at 0.3 MPa, and the droplet size was tested at different spray heights h and electrostatic voltage U. The test results are presented in Figure 26. The results show that droplet size gradually decreased when the spray height h and electrostatic voltage U increased. When the spray height h was 1m and the electrostatic voltage U was 18 kV, hence, the droplet size reaches at a minimum value of 18.4 μm. The main reason for that is when the droplets just missed out from the nozzle, the particle size showed great changes takes place. However, when jet distance atomized droplets, the charged droplets will be broken in under the action of electrostatic field, and further at the same time, due to the Coulomb force between charged droplets effects, it makes the particle size diameter smaller.

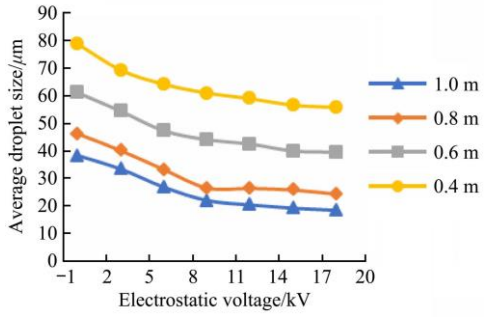

Figure 26 Variation of droplet size under different spray heights and electrostatic voltages

8 Conclusions

The following conclusions were drawn from the experimental based study:

(1) Through range analysis of the simulation results, it was found that when the included angle θ of the two-stage resonator was 80°, the diameter d of the resonator was 4.86 mm, and the length ratio of L_1/L_2 was 1, then the resonant frequency f of the two-stage resonator at this stage was largest and its atomization performance was also the best. Moreover, when the included angle between the two stage resonators was 80°, the diameter d was 4.86 mm, the tube length ratio was 1.0, and the gas pressure was 0.5 MPa, the droplet size reached 22.0 μm, while the included angle increased to 90°, the droplet size was calculated 59.67 μm, the droplet size reduced by 63%.

(2) The charging electrode of the electrostatic induction part was selected, and the electric field distribution around the electrode ring was analyzed. The optimal charge range of the electrode ring as the axial distance was less than 20 mm.

(3) Comsol Multiphysics, a multi-physical field coupling analysis software was used based on phase field method of droplet deformation and broken condition. It was simulated and analyzed through the comparative analysis of different electrostatic voltage U, and surface tension σ. The shape of the droplet variable was proportional to the electrostatic voltage U. However, it was inversely proportional to the surface tension σ, and directly proportional to the droplet diameter d. Moreover when the voltage reached to a certain saturation value, the water droplets breaks up.

(4) By the different spray height, electrostatic voltage and gas pressure of each test, the experimental results showed that the particle diameter and gas pressure P_0, electrostatic voltage U, spray height h are inversely proportional to each other. When the gas pressure was 0.4 MPa, electrostatic voltage was 18 kV, particle size diameter of 7.8 μm, and in other condition, the voltage applied was 0 kV, and particle diameter decreased by 82.2% and reached to 43.9 μm.

Acknowledgements

This work was financially supported by National Natural Science Foundation of China Program (Grant No. 51975255), Jiangsu Agriculture Science and Technology Innovation Fund (Grant No. CX (18) 3048), and Priority Academic Program Development of Jiangsu Higher Education Institutions (Grant No. 37(2014)).

[References]

[1] Moges G, Mcdonnell K, Delele M A. Backpack magnetic sprayer:off-target drift and on-target deposition uniformity in a sugarcane plantation. Int J Agric & Biol Eng, 2021; 14(6): 27–36.

[2] Li H, Niu X X, Ding L, Tahir A S, Guo C L, Chai J J, et al. Dynamic spreading characteristics of droplet impinging soybean leaves. Int J Agric & Biol Eng, 2021; 14(3): 32–45.

[3] Zhang W, Hou Y R, Liu X, Lian Q, Fu X M, Zhang B, et al. Wind tunnel experimental study on droplet drift reduction by a conical electrostatic nozzle for pesticide spraying. Int J Agric & Biol Eng, 2017; 10(3): 87–94.

[4] Basu S, Luthra J, Nigam K. The effects of surfactants on adhesion, spreading, and retention of herbicide droplet on the surface of the leaves and seeds. Journal of Environmental Science & Health. Part. B Pesticides Food Contaminants & Agricultural Wastes, 2002; 37(4): 331–344.

[5] Yi H, Huang J, Gu X, Ni Z. Study on ultrasonic spray technology for the coating of vascular stent. Sci. China Technol. Sci., 2011; 54(12): 13.

[6] Okawa H, Nishi K, Dai S, Kawamura Y. Influence of air humidity and water particles on dust control using ultrasonic atomization. Japanese Journal of Applied Physics, 2012; 51(7S): 07GE06. doi: 10.1143/JJAP.51.07GE06.

[7] Barba A A, Amore M D', Cascone S, Lamberti G, Titomanlio G. Intensification of biopolymeric microparticles production by ultrasonic assisted atomization. Chemical Engineering & Processing Process Intensification, 2009; 48(10): 1477–1483.

[8] Yasuda K, Honma H, Xu Z, Asakura Y, Koda S. Ultrasonic atomization amount for different frequencies. Japanese Journal of Applied Physics, 2011; 50(7): 07HE23. doi: 10.1143/jjap.50.07he23.

[9] Annalisa D, Angela B A, d'Amore M. Analysis of size correlations for

microdroplets produced by ultrasonic atomization. The Scientific World Journal, 2013; 2013: 482910. doi: 10.1155/2013/482910.

[10] Song K T, Gao J M. Design and simulation of focused low-frequency ultrasonic atomizing nozzle. Journal of Agricultural Mechanization Research, 2013; 4: 63–66. (in Chinese)

[11] Gao J M, Li Y B, Ren N. Design and simulation of a novel low-frequency ultrasonic atomizing nozzle based on focuzing ultrasinic levitation. National Symposium on Piezoelectricity, Acoustic Waves, and Device Applications, IEEE, 2010.

[12] Shiau Y J, Chu C Y. Comparative effects of ultrasonic transducers on medium chemical content in a nutrient mist plant bioreactor. Scientia Horticulturae (Amsterdam), 2010; 123(4): 514–520.

[13] Lakhiar I A, Liu X D, Wang G Q, Gao J M. Experimental study of ultrasonic atomizer effects on values of EC and pH of nutrient solution. Int J Agric & Biol Eng, 2018; 11(5): 59–64.

[14] Thomas M E, Disalvo R, Makar P. Electrostatic atomization insertion into compression ignition engines. SAE Technical Paper, 2002. doi: 10.4271/2002-01-3053.

[15] Liu C J, Wang K Y. Gas-assisted electrostatic nozzle atomization performance and charging effect experiment. Journal of Zhejiang Forestry College, 2009; 26(1): 116–121. (in Chinese)

[16] Gao J M, Ma J L. Design and test of low-frequency Hartmann atomization nozzle with stepped resonance tube. Transactions of the CSAE, 2017; 33(12): 66–73. (in Chinese)

[17] Hou Y R. Mechanism of atomization and experimental study on agricultural aviation electrostatic spraying nozzles. Master thesis, Heilongjiang Bayi Agricultural University, 2017; 80p. (in Chinese)

[18] Li J L. Simulation of Electrohydrodynamic atomizated droplet trajectory and experiment research of deposition. Master Thesis, Dalian University of Technology, 2013; 70p. (in Chinese)

[19] Liang M, Li Q, Wang K S, Liu J Y, Chen J Q. Deformation and breakup of dispersed phase droplets in uniform electric field. Journal of Chemical Industry, 2014; 65(3): 843–848. (in Chinese)

[20] Yang C, Chen B, Jiang W L, Gao D R, Jin G J. Analysis and experiment on atomizing characteristics of supersonic nozzle based on Laval effect. Transactions of the CSAE, 2016; 32(19): 57–64. (in Chinese)

[21] Wang K Y, Han X X, Zhang X T, Liu Y P, Chen J C. Design and simulation on scaling supersonic nozzles. Chinese Journal of Construction Machinery, 2011; 9(3): 304–308. (in Chinese)

[22] Yuan Z H. Calculation and analysis of airflow state parameters in Laval nozzle. Technology Information, 2018; 16(13): 30–35.

[23] Wang J G. Nozzle design research. Heavy Machine, 1981; 8: 46–53, 61. (in Chinese)

[24] Li B, Hu G H, Zhou Z W. Numerical simulation of flow field of Hartmann resonance tube and supersonic atomizing nozzle. Applied Mathematics and Mechanics, 2007; 28(11): 1261–1271. (in Chinese)

[25] Qiu Y B. Test design and data processing. China University of Science and Technology Press, 2008. (in Chinese)

[26] Lu J J, Chen J D, Wu Y D, Wang B. Agricultural aviation research aeronautical electrostatic spray system performance. Mechanization Research, 2019; 41(12):174–179. (in Chinese)

[27] Zhou L F, Zhang L, Xue X Y, Chen C. Research progress and application status of pesticide electrostatic spray technology. Transactions of the CSAE, 2018; 34(18): 1–11. (in Chinese)

[28] Zheng T Y. Research on crude oil emulsion demulsification and water droplet dynamic characteristics under electric field. Master thesis, Harbin University of Science and Technology, 2015; 61p. (in Chinese)

[29] Taylor G I. The formation of emulsions in definable fields of flow. Proceedings of the Royal Society A: Mathematical, Physical and Engineering Sciences, 1934; 146(858): 501–523.